Talanta 122 (2014) 201–208

Contents lists available at ScienceDirect

Talanta

journal homepage: www.elsevier.com/locate/talanta

H_2 sensing properties of two-dimensional zinc oxide nanostructures

Matteo Tonezzer [a,*], Salvatore Iannotta [b]

[a] IMEM CNR, sede di Trento - FBK, Via alla Cascata 56/C, Povo - Trento, Italy
[b] IMEM CNR, Parco Area delle Scienze 37/A, I-43124 Parma, Italy

ARTICLE INFO

Article history:
Received 20 August 2013
Received in revised form
15 January 2014
Accepted 20 January 2014
Available online 31 January 2014

Keywords:
Nanostructure
Zinc oxide
Gas sensor
Hydrogen

ABSTRACT

In this work we have grown particular zinc oxide two-dimensional nanostructures which are essentially a series of hexagonal very thin sheets. The hexagonal wurtzite crystal structure gives them their peculiar shape, whose dimensions are few microns wide, with a thickness in the order of 25 nm. Such kind of nanostructure, grown by thermal oxidation of evaporated metallic zinc on a silica substrate, has been used to fabricate conductometric gas sensors, investigated then for hydrogen gas detection. The "depletion layer sensing mechanism" is clarified, explaining how the geometrical factors of one- and two-dimensional nanostructures affect their sensing parameters. The comparison with one-dimensional ZnO nanowires based structures shows that two-dimensional nanostructures are ideal for gas sensing, due to their tiny thickness, which is comparable to the depletion-layer thickness, and their large cross-section, which increases the base current, thus lowering the limit of detection. The response to H_2 has been found good even to sub-ppm concentrations, with response and recovery times shorter than 18 s in the whole range of H_2 concentrations investigated (500 ppb–10 ppm). The limit of detection has been found around 200 ppb for H_2 gas even at relatively low working temperature (175 °C).

1. Introduction

Gas sensors are needed in a broad range of applications: homeland security, industrial safety, automotives, medical diagnosis, environmental monitoring etc. [1]. Hydrogen (H_2) is one of the most useful gases, being used in many chemical processes and various fields including aerospace, medical, petrochemical, transportation, and energy [2–5]. In recent years, H_2 has attracted a large amount of attention as a prospective clean energy source. However, it is a low molecular weight gas and can easily leak out and may cause fires or explosions. Furthermore, hydrogen gas is tasteless, colorless and odorless so it cannot be detected by human beings. Its low ignition energy and wide flammable range make it easily inflammable and explosive. Therefore rapid and accurate hydrogen detection is necessary during the production, storage and use of hydrogen. In the scenery of gas-sensing technologies, conductometric metal-oxide gas sensors are widely used due to their high and fast response and simple device structures that allow portable applications [6,7]. Since the work of Seiyama [8], many scientists investigated the sensing properties of different metal oxides for different gases, trying to find the best materials and architectures. Zinc oxide, one of the most studied metal oxides is a multifunctional semiconductor among the most promising materials for gas sensor applications [9,10], also for its stability, safety and biocompatibility [11]. ZnO gas sensors were in the past fabricated in the form of pellets or thick films. An improvement was then obtained using thin films. Indeed, in comparison with conventional sintered bulk gas sensors, thin film gas sensing materials have better performance. More recent research has been devoted towards zinc oxide nanoparticles, since reactions at grain boundaries and complete depletion of carriers in the particles can modify more strongly the conductivity. Unfortunately, the high temperature required for the surface reactions to take place induces a grain growth by coalescence and avoids the achievement of stable conditions [12,13]. For this reason the latest research focused on nanowires and nanorods, that combine tiny dimensions similar to the depletion layer thickness [14,15] and a much better thermal stability. Such kind of quasi-one-dimensional nanostructures reach good response values, but usually the low base current does not permit them to have a good limit of detection (LoD), which is a very important parameter for applicative sensors. For example, Hassan and coworkers have investigated vertical and oblique ZnO nanorods as hydrogen gas sensor, obtaining good response values, but long response and recovery times (176 and 116 s, respectively), and a LoD of 150 ppm [16]. Other recent papers are compared with present results along the paper (see Tables 1 and 2). To our knowledge, no works have been focusing yet on two-dimensional nanostructures. In this work, we report the growth of zinc oxide nanohexagones: wide hexagonal sheets which are few microns wide and around 25 nm thick. Such kind of nanostructure is useful for investigating how two-dimensional nanostructures compared to

* Corresponding author. Tel.: +39 0461 314828; fax: +39 0461 314875.
E-mail addresses: matteo.tonezzer@cnr.it, matteo_tonezzer@yahoo.it (M. Tonezzer).

0039-9140/$ - see front matter © 2014 Elsevier B.V. All rights reserved.
http://dx.doi.org/10.1016/j.talanta.2014.01.051

one-dimensional counterparts (nanowires) when used in gas sensing applications. The depletion layer modulation model affects differently the geometries of one- and two-dimensional nanostructures, influencing their sensing performance. It will be shown that a lower sensor response is balanced by a better limit of detection.

2. Materials and methods

2.1. Nanostructures growth

A two-step process has been used to grow the nanohexagones: a thermal evaporation of pure metallic zinc ($\geq$ 99.99%, Sigma-Aldrich) onto a Si/SiO_2 substrate (Siltronix), followed by the thermal oxidation in a horizontal furnace (Lingdberg Blue M). The Si/SiO_2 wafer (thermally deposited SiO_2 was 300 nm thick) was cut in small $10 \times 10\ mm^2$ substrates and deposited with around 200 nm of pure zinc. After that the zinc-deposited substrates were loaded in an alumina boat. The boat was then introduced in a quartz tube inserted in a horizontal furnace connected to a vacuum system. The whole apparatus was evacuated at its limit pressure (around 5×10^{-4} mbar) and purged with nitrogen (99.9999%, SIAD) three times. After that a mixture of oxygen (5%) in nitrogen was flown inside the quartz pipe through a valve, and the pressure was maintained at 5 mbar. The thermal oxidation process was then carried out rising the temperature to its maximum in 15 min, maintaining it for 2 h, and then cooling down slowly. The substrates were positioned in the center of the furnace and the temperature was chosen in a range from 75 to 350 °C, with an error of less than ± 0.5 °C. The temperature calibration inside the tube was achieved by scanning a thermocouple along the length of the tube under flow and temperature identical to those of the growth conditions. The samples, once taken out of the quartz pipe, showed a very light gray cover, composed of zinc oxide nanostructures. The optimization of the growth parameters gave as a final result hexagonal two-dimensional nanosheets which show a large surface/volume ratio because of its nano-on-microstructure. Changing the parameters we would obtain different ZnO nanostructures like nanorods, nanoblades, nanowires etc.

2.2. Nanostructures characterization

Scanning electron microscopy (SEM), transmission electron microscopy (TEM), X-ray diffraction (XRD), energy-dispersive X-ray spectroscopy (EDS) and X-ray photoelectron spectroscopy (XPS) analysis were used to characterize respectively the morphological, structural and compositional properties of the hexagonal nanostructures. Field emission scanning electron microscopy (FE-SEM) analysis was carried out using a Jeol JSM-7001F operated at 15 kV. Fig. 1a shows a scanning electron micrograph of the ZnO nanohexagones, evidencing their uniformity and size homogeneity. Nanohexagones are wide (few microns in diameter), thin (around 25 nm thick) and present a homogeneous porosity. Transmission electron microscopy was performed using a Tecnai G2 SuperTwin, operated at 200 kV. Fig. 1b shows a high resolution image (HR-TEM) of a nanohexagon edge, in which the lattice fringes are clearly visible, proving the good crystallinity of the nanostructures. XRD spectra were collected in Bragg–Brentano geometry with a PANalytical X'Pert Pro diffractometer. A Cu anode with wavelength of 1.5406 Å was used. The step size was 0.05° (2Θ) and the average time was 60 s/step. Fig. 2a shows a typical XRD pattern in logarithmic scale. The well defined peaks (sharp and intense in linear scale) confirm the good crystalline nature the nanostructures as wurtzite (hexagonal) ZnO with lattice constants of $a = 3.249$ Å and $c = 5.206$ Å, consistent with the standard values in the standard data (JCPDS 36-1451 card). The comparison between the standard card and the experimental spectrum shows a very intense peak originated from (002) reflection, which identifies it as the preferred growth direction of the sheets.

Peaks of relatively low intensities ($< 10\%$) corresponding to (100), (101), (102), (110), (103), (200), (112) and (201) planes are also present. No extra peaks related to any impurity were observed. This confirms that the as-synthesized ZnO nanostructures are pure wurtzite-type ZnO. The texture coefficient as a function of the lattice direction is shown in Fig. 2b, where the high directionality of the spectrum can be easily noticed. The texture coefficient has been calculated to describe the preferential orientation (hkl) using the following expression [17]:

$$T_C = \frac{I(hkl)/I_0(hkl)}{1/\sum_N I(hkl)/I_0(hkl)} \quad (1)$$

where N is the number of diffraction peaks, $I(hkl)$ and $I_0(hkl)$ are, respectively, the measured and corresponding recorded intensities according to JCPDS (36-1451) card. The value of the texture coefficient indicates the maximum preferred orientation of the films along the diffraction plane.

Fig. 3 reports a typical EDS spectrum, which identifies the nanostructures material as ZnO with a good stoichiometry (O: 49 ± 1 at%/Zn: 51 ± 1 at%).

Elemental compositions and purity of ZnO nanohexagones were also studied by XPS analysis. XPS measurements were performed VG ESCA LAB MK II spectrometer using Al Kα (1486.6 eV) radiation from an X-ray source operated at 12 kV, 10 mA. The binding energies in all the XPS spectra have been calibrated using that of C 1s (284.6 eV). High resolution spectra for Zn and O are shown in Fig. 4(a) and (b). The spectrum in Fig. 4(a) shows two significant binding energy peaks at 1021.9 and 1044.9 eV corresponding to the electronic states of Zn 2p3/2 and Zn 2p1/2 respectively. The energy difference between these two peaks is 23.04 eV, which agrees well with the standard value of 22.97 eV [18]. The O 1s peak is located at 530.6 eV. The spectrum shows an intensity asymmetry towards high energy. This could be explained by a lower oxygen presence, due to a superficial deviation from stoichiometry. The Zn/O ratio was calculated by selecting the Zn 2p3/2 and O 1s line peaks. All the samples showed values in the range 1.9–2.2. Both XRD and XPS measurements confirm that nanohexagones are pure ZnO.

2.3. Gas sensing experiments

Gas sensing properties of the ZnO nanohexagones were tested in a home-built apparatus including a test chamber, a sensor holder which could be heated up to 500 °C, mass flow controllers (connected to high purity calibrated bottles), a Keithley 2410 multimeter, a Keithely 6517A electrometer, and a data acquisition system (LabView, National Instruments). To achieve a good contact for the electrical measurements, two thin electrodes of pure gold ($> 99.99\%$, Sigma Aldrich) were thermally evaporated through a shadow mask letting a channel of 50 microns between the two "pads". The gold electrodes were then contacted via two passive micromanipulators.

The device was first biased with 1 V voltage and operated in a temperature-controlled atmospheric pressure of dry air (79% nitrogen, 21% oxygen). A voltage ranging from -1 V to $+1$ V has been applied to the sensors in different hydrogen concentration conditions, at room temperature. A very good ohmic behavior can be observed in Fig. 5, which is necessary to the sensing properties since the response of a gas sensor can be maximized when the metal–semiconductor junction is ohmic or has a negligible junction resistance.

The resistance of the sensors was in the 100–800 kΩ range under dry air atmosphere at 75–350 °C. Before starting the measurements, the gas sensors underwent a thermal conditioning at 350 °C at 1 V in

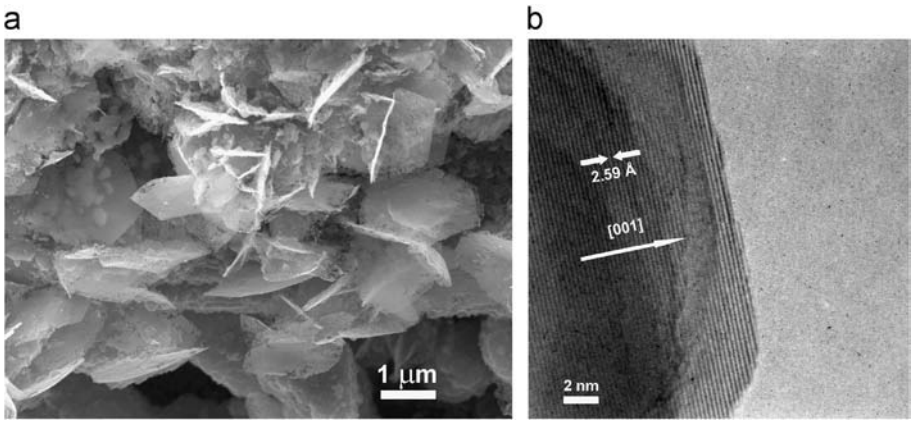

Fig. 1. Electron microscopy images of the samples. (a) SEM image of the ZnO nanohexagones forest; and (b) TEM image of a single nanostructure.

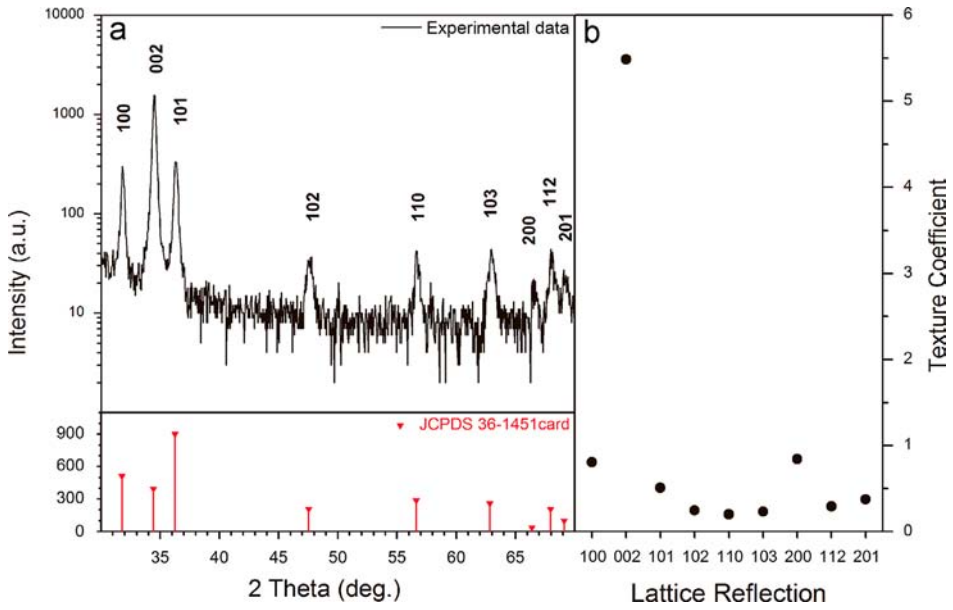

Fig. 2. (a) Logarithmic scale XRD pattern of the ZnO nano-hexagones with a standard reference (red lines); and (b) texture coefficient evidencing the preferential orientation of the nanostructures. (For interpretation of the references to color in this figure legend, the reader is referred to the web version of this article.)

dry air (500 sccm in total, 79% nitrogen, 21% oxygen) for 5 h, to make their microstructure steady and thus improve the repeatability of the tests. Such a conditioning balanced indeed the presence of oxygen adatoms on the ZnO nanohexagones surfaces, thus stabilizing the standard depletion layer [19]. The sensing performance of the ZnO devices are investigated with an operating voltage of 1 V between the electrodes.

3. Results

3.1. Working temperature

The first experiment was investigating the response of the sensors as a function of the working temperature in the range from 75 °C to 350 °C. The best working temperature is indeed an important parameter for such a kind of gas sensor, mainly because of the power consumption needed to heat it up. The sensor temperature was thus controlled by a feedback on the thermocouple inside the sensing chamber. The resistance of the sensors in dry air or in test gases could be measured monitoring the output current across the sensor.

Fig. 6 shows the response of the ZnO nanohexagones-based gas sensor to 500 ppm of hydrogen, as a function of working temperature. It shows the influence that working temperature has on the response of the sensor for 500 ppm of hydrogen in dry air. The sensor response exhibits a peak at 175 °C, with a response value of 5.37. In this paper we use the definition of sensor response, as $S_R = R_{air}/R_{H_2}$ where R_{air} and R_{H_2} are, respectively, the resistance of the nanowires exposed to dry air without and with hydrogen gas.

As can be seen in Fig. 6, the sensors response starts under 100 °C but their response greatly improves over 150 °C, reaching a relative maximum at 175 °C, with the highest response value of 5.37 for 500 ppm H_2 in dry air. For the previously mentioned considerations, 175 °C has been chosen as the working temperature.

The optimal operating temperature of nanohexagones hydrogen sensors (175 °C), revealed by response measurements at different temperatures, fully matches with the transition temperature at which some kind surface states are replaced with others.

This bell shaped dependence of sensor response on working temperature appears due to two competing processes: (a) the reaction of hydrogen gas with oxygen centers O^- on the surface of the zinc oxide, leading to the increase of conductivity, and (b) gas

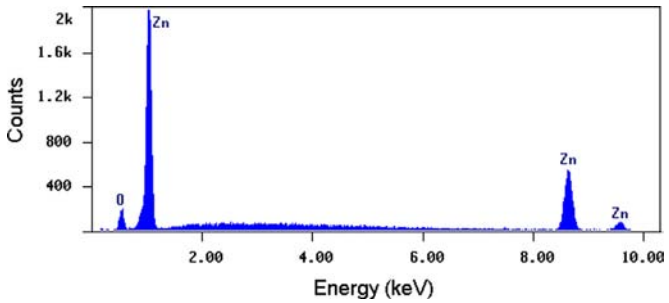

Fig. 3. Compositional analysis: EDS pattern of the nano-hexagones, confirming the presence of only O and Zn and the good stoichiometry of the ZnO nanostructures.

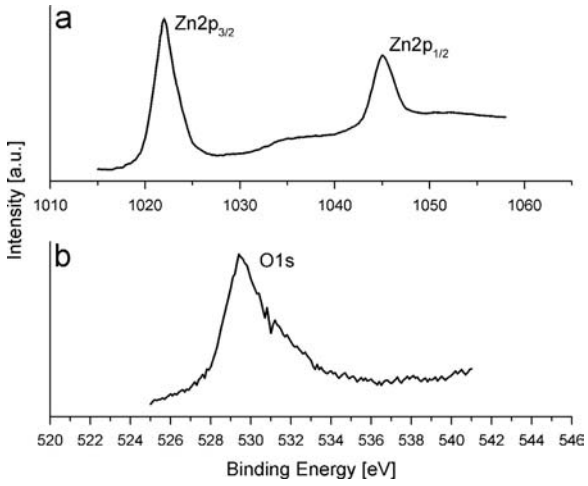

Fig. 4. XPS spectra of zinc and oxygen, showing a superficial deviation from stoichiometry.

desorption from its surface. So long as the reaction rate constant rises along with temperature, the equilibrium concentration of gas on the surface of the metal oxide nanostructures decreases due to an increase in the desorption rate [20–22].

3.2. Hydrogen response

All the experiments have been implemented at 175 °C, as it has been found the optimal working temperature for such kind of sensing devices (good balance between sensor performance and low temperature, meaning low power consumption and wider usability). The devices have been tested with different concentrations of hydrogen gas in dry air, ranging from 500 ppb to 500 ppm (see Fig. S1 in Supporting information). Fig. 7 shows the response and recovery of ZnO nanohexagones upon exposure to 0.5, 1, 2, 5, and 10 ppm hydrogen at the work temperatures of 175 °C (dynamic change of current is shown in Fig. S2 in Supporting information).

In the absence of hydrogen gas flow in the chamber, the resistance measured was high and steady. However, when hydrogen gas was injected in the chamber, the resistance of the sensor changed abruptly.

It is also observed that the response increases linearly as a function of hydrogen concentration in the measured range (up to 500 ppm). The initial resistance is steady, and the response and recovery is rapid. As indicated by Fig. 7, the fabricated sensors show a clear and fast resistance change even to 500 ppb hydrogen. It is known that semiconducting oxide gas sensors operate on the basis of the electrical properties variations of an active element, triggered by the adsorption of an analyte on the surface of the sensor.

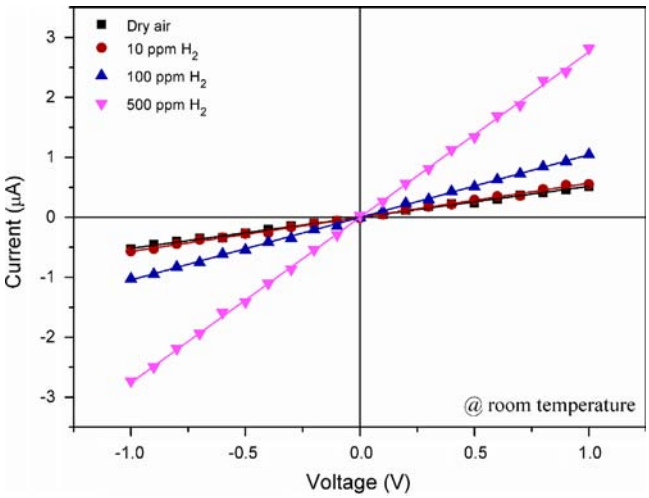

Fig. 5. Typical *I–V* curves of the nanohexagones sensors in dry air and in different concentrations of hydrogen.

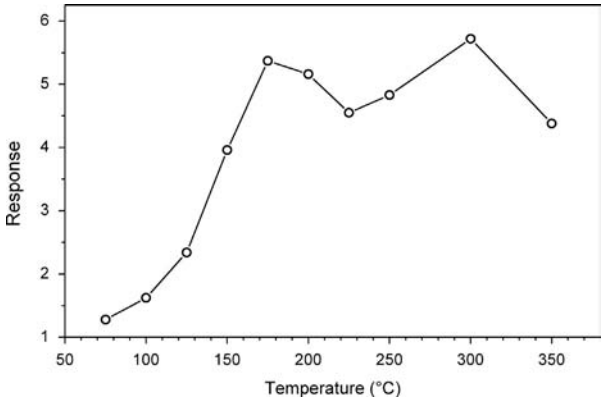

Fig. 6. Sensor response of the ZnO nano-hexagones devices to 500 ppm H_2 as a function of working temperature.

When a ZnO nanostructured sensor is exposed to air, an O_2 molecule adsorbs on the surface of the ZnO nanostructures and forms an O_2^- ion by draining an electron from its conduction band. Thus, ZnO nanostructures show a high resistance state in air ambient. When the ZnO nanostructured sensor is exposed to a reductive gas like hydrogen at moderate temperature, the gas reacts with the surface oxygen species, which decreases the surface concentration of O_2^- ions and increases the electron concentration. This in the end raises the conductivity of the ZnO nanostructures. In the case of ceramic or film, the electrical alteration only takes place in the grain boundary or porous surface. In the case of narrow ZnO nanostructures, it is expected that the electronic transport properties of most of the nanostructure section will change. The large portion of the nanostructure section which is depleted of charge carriers explains why ZnO nanostructures always show higher sensing performance compared to thin film or bulk sensors. The inset in Fig. 7 shows a zoom of the curve, in order to better illustrate the complete response and recovery of the sensor, and give a qualitative view of the response and recovery times. A comparison of present results with recent literature is reported in Table 1. Response and recovery times will be better discussed in a subsequent section.

As can be seen in Table 1, the sensor response of nanohexagones-based devices is comparable but not higher than the values found for one-dimensional nanowires and nanorods working at a similar

Table 1
Gas response values at different H_2 concentrations, from different recent papers.

H_2 concentration (ppm)	Working temperature (°C)																				
	300	200	200	200	250	RT	250	175	225	25	25	25	25	25	150	300	400	25	150	200
0.5								**1.007**												
1								**1.012**												
2								**1.024**												
5								**1.044**						0.12						
10								**1.089**												
20														0.17						
40														0.18						
50				2.6				**1.572**	50											
60				3.1																
80				4.6								0.37	0.34		10					
100				5.3				**2.043**			0.01			0.22						
150	3.2						8.5	**3.021**		0.04										
200	4.5	1.45			1.019			**5.370**								0.18				
500	7.0	1.59	2.2		1.025	1.39								0.30		0.43	7.6			
1000		1.78				1.79														
1500					1.044	1.92														
2500																				
20000																		0.42	1.4	1.75
Ref.	[23]	[24]	[25]	[26]	[27]	[28]	[29]	**Present work**	[30]	[31]	[32]	[33]	[34]	[35]	[8]	[36]	[37]	[38]		
Year	2009	2009	2011	2010	2010	2010	2006		2013	2008	2007	2012	2010	2013	2013	2006	2010	2013		

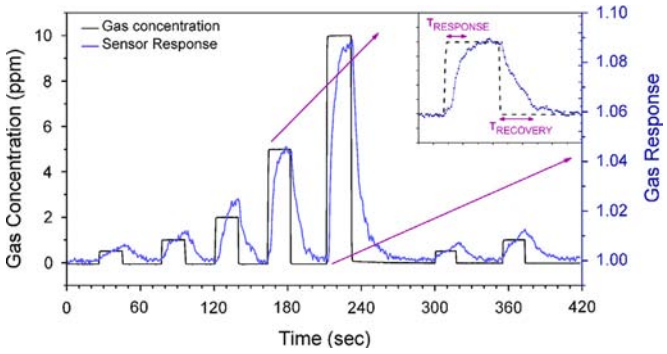

Fig. 7. Dynamic response of ZnO nano-hexagones sensors working at 175 °C while different concentration of hydrogen are injected and evacuated. The zoom in the inset shows the response and recovery times calculation.

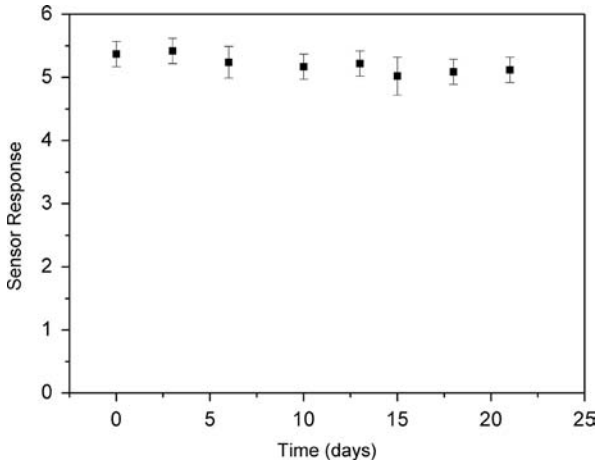

Fig. 8. Sensor response as a function of time along a three weeks period. The sensor was tested in dry air with 500 ppm H_2 at 175 °C.

operating temperature, as expected from geometrical considerations on its cross-section.

3.3. Response reversibility

The initial thermal annealing at a high temperature in dry air renders the nanohexagones systems very stable [39]. Their responses are, thus, reversible and reproducible even during different gas cycles, as shown in Fig. 7.

Reproducibility was observed as second pulses of 500 ppb and 1 ppm hydrogen gas were introduced into the sensor chamber. It was found that the ZnO nanohexagones-based sensor produce repeatable responses of the same magnitude with good baseline stability. Response reversibility is a very important but under-evaluated parameter, because a low reversibility means a high drift in the sensor response, which makes harder its usage and real application. In order to evaluate the reversible degree of a sensor response, the *percentage recovery degree* $\%R$ will be used in this work, where $\%R=(R-I)/I \times 100$ and I is the response intensity. The sensors investigated showed a maximum $\%R$ of 4% in the worst condition (500 ppb response). Such a small value proves the good performance of the sensors over time. The sample resistance and the sensor response have been tested over a 3 weeks period in ambient air at 175 °C, as shown in Fig. 8.

There is no evidence that the sensors based on ZnO nanohexagones suffer from long-term drift of resistance or a performance degrading in our experiments. Such good reversibility and stability values are very important for the gas sensor to be used in real world practical applications.

3.4. Response and recovery times

It is well known that response and recovery behavior is an important characteristic for evaluating the performance of gas sensors.

The response time has been here defined as the time required for the response to reach 90% of the equilibrium value after hydrogen gas was injected, and the recovery time was the time necessary for a sensor to attain a response 10% above its original value in dry air. As can be seen in Fig. 9, the response times ranged from 7.5 s for 5 ppm to 17.5 s for 500 ppb. The recovery times were a bit longer, ranging from 11.5 s for 5 ppm to 17.5 s for 500 ppb. These times are the result of an intrinsic convolution of the sensor response time and the test chamber filling and evacuating time. In our case, considering the test chamber volume of 50 cm^3 and the

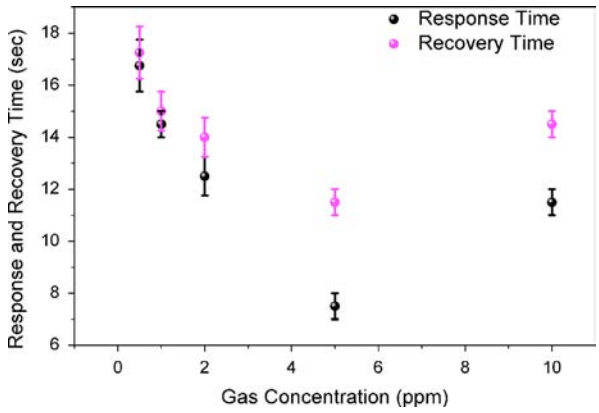

Fig. 9. Response and recovery times as a function of hydrogen concentration, measured at 175 °C.

Table 2
Response times at different H_2 concentrations, from different recent papers.

Hydrogen concentration (ppm)	Working temperature (°C)							
	200	200	200	200	250	RT	250	175
0.5								16.75
1								14.5
2								12.5
5								7.5
10								11.5
50				15				
60				13				
80				11				
100				9				
200	90						200	
500	62	48			300			
1000	34	51	257		427	498		
1500		40				415		
2500					387	395		
Reference	[20]	[21]	[22]	[23]	[24]	[25]	[26]	Present work

inlet gas flow of 500 sccm, a filling time of 6 s can be calculated. This time is shorter than the response times obtained for the total system (sensor plus test chamber), meaning that the sensors response times would be even shorter. The *V* behavior of response and recovery times in Fig. 9 can be ascribed to a competition between two processes. A higher concentration of gas molecules in the same sensing chamber volume can favor a faster response time, because a higher metal oxide surface is affected by the gas molecules reactions. When the concentration reaches a threshold (which depends on the specific system characteristics), the diffusion rate of the gas molecules becomes more important and can limit the overall sensing reaction speed.

These time periods were much shorter compared with the average times for nanowires-based devices from recent literature, as can be seen in Tables 2 and 3. Their rapid responses and recoveries even at very low hydrogen concentrations make nano-hexagones the ideal choice for real-time sensing in many fields and applications.

When reducing gases like hydrogen are detected using n-type oxide semiconductor gas sensors, the recovery time values are usually longer than the response time values [40,41]. This can be seen also comparing the respective values in Tables 2 and 3, where the recovery times are slightly slower than response times, and can be explained by the noticeably slower series surface reactions to form O^- adatoms during the recovery, compared to the oxidation reaction of reducing gas by O^- ads. In pure ZnO, a series of reactions are necessary for the recovery, as following:

Table 3
Recovery times at different H_2 concentrations, from different recent papers.

Hydrogen concentration (ppm)	Working temperature (°C)							
	200	200	200	200	250	RT	250	175
0.5								17.25
1								15
2								14
5								11.5
10								14.5
50				101				
60				100				
80				98				
100				85				
200	> 480						800	
500	> 300	80			747			
1000	> 420	91	632		729	332		
1500		74				373		
2500					855	402		
Reference	[20]	[21]	[19]	[20]	[21]	[22]	[23]	Present work

(1) desorption of H_2O, (2) diffusion of oxygen to the sensing surface, (3) adsorption of oxygen gas, (4) dissociation into atomic oxygen on the surface, and (5) ionization to negative charge of surface oxygen (O^- ads).

3.5. Sensitivity

As can be qualitatively noticed in Fig. 7 (and in better detail in Fig. S3, in Supporting information), the sensor response increases linearly in the 0–2 ppm range and then starts to decrease. The first derivative, or slope, of the curve in Fig. S3 gives the sensitivity value.

In our case, the sensor sensitivity was 0.012 ppm^{-1} up to 2 ppm and then it decreases to 0.008 ppm^{-1} in the range 2–10 ppm. This indicator has an important meaning: it indicates how precise can be the sensor in giving the analyte concentration.

3.6. Limit of detection

Along the lowest H_2 concentration tested, the current variation increases linearly from zero to 2 ppm as a function of the H_2 concentration (Fig. S3, in Supporting information), and then starts to be slightly less sensitive. Using a linear fit on the initial part of the curve, and taking into account that the current noise is about 1.34×10^{-3} μA (a definition of three times the standard deviation σ of the signal has been used in this work), an hydrogen limit of detection (LoD) lower than 200 ppb is obtained. Such small LoD value allows to detect a leak at the beginning, and is very significant in a range of applications related to safety. This value is low if compared with one-dimensional ZnO nanostructures. Even if this parameter is not often investigated, ZnO nanowires and nanorods based sensors usually show LoD values that go from few to some tens of ppm [42–44].

3.7. Adsorption and desorption kinetics

The diffusion of hydrogen gas on the two-dimensional porous ZnO nano-hexagones during the gas-sensing process was further investigated from the point of view of gas adsorption and desorption kinetic processes. As already demonstrated, the sensing mechanism of ZnO is obviously based on surface reactions. Thus, the gas adsorption and desorption processes can be studied in terms of the kinetics of the modifications on the surface of semiconducting material. In other words, the change of the sensor current can be used to inspect the surface state of sensing materials during adsorption or desorption process. In our

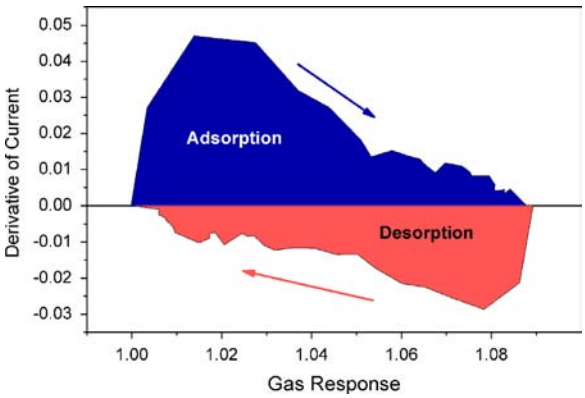

Fig. 10. Complete gas adsorption and desorption cycle, showing the speed of surface processes.

investigations, the dynamic response and current curves were mathematically transformed. Taking the response of the gas sensor towards 10 ppm hydrogen as an example, the dynamic sensor response was defined as *x*-axis, while the derivative of current towards time was transformed as *y*-axis, as shown in Fig. 10.

Fig. 10 shows a complete gas adsorption and desorption cycle. When hydrogen gas is injected into the detection chamber, its adsorption on the ZnO nanohexagones dominates the initial sensing process. The initial sharp peak indicates that the adsorption process reaches its maximum speed very quickly.

Once the surface reactions between hydrogen and oxygen are balanced to a new equilibrium, the adsorption process ends (right part of the curve). When the hydrogen gas is evacuated, its surface desorption and the adsorption of oxygen dominate the surface processes giving rise to a negative slope that is here reflected in the sharp negative peak on the right in Fig. 10. Again, a sharp peak confirms that the desorption process is fast in achieving its highest speed. Both adsorption and desorption processes indicate that the two-dimensional porous structure of ZnO nanohexagones makes them ideal candidates for fast gas-sensing devices fabrication.

4. Discussion

Although the precise basic mechanisms that cause metal oxide gas response are still disputed, it is known that a change in conductivity comes from the trapping of electrons at adsorbed molecules and band bending induced by these chemisorbed molecules. Typically, oxygen molecules are adsorbed on the surface of the ZnO sensing material in air. The adsorbed oxygen species can drain electrons from the core of the ZnO nanostructure. These oxygen species trap negative charge causing a depletion layer and thus a decreased conductivity. When the sensing material is exposed to a reducing gas, the electrons trapped by the oxygen adsorbates will return to the ZnO structure core, leading to an increase in conductivity. The electrical conductance of ZnO nanostructures is influenced by the presence of oxidizing gases due to two successive reactions occurring on their surface [45]. In the first reaction atmospheric oxygen molecules, which are physisorbed on the surface sites (Eq. (2)), are ionized during their movement on the surface, by capturing electrons from the conduction band, thus becoming ionosorbed (Eqs. (3–5)).

With increasing temperature, the state of oxygen adsorbed on the nanostructures surface is subjected to the following reactions [46]:

$$O_{2\ (gas)} \leftrightarrow O_{2\ (adsorbed)} \quad (2)$$

$$O_{2\ (adsorbed)} + e^- \leftrightarrow O_{2\ (adsorbed)}^- \quad (3)$$

$$O_{2\ (adsorbed)}^- + e^- \leftrightarrow 2O^-_{\ (adsorbed)} \quad (4)$$

$$O^-_{\ (adsorbed)} + e^- \leftrightarrow O^{2-}_{\ (adsorbed)} \quad (5)$$

The above equations show that electrons are consumed in the reactions, and explain the resistance increase after the O_2 exposure.

When the ZnO nanostructure is exposed to a reducing test gas such as hydrogen, its atoms react with these chemisorbed oxygen ions and produce H_2O molecules consuming chemisorbed oxygen from the metal oxide surface by releasing electrons. As a result electrons will be released back to the conduction band and will contribute to current increase through the nanohexagones. This also results in a reduction of surface depletion region and increase conductivity.

$$H_{2\ (gas)} \leftrightarrow H_{2\ (adsorbed)} \quad (6)$$

$$H_{2\ (adsorbed)} + O^-_{\ (adsorbed)} \rightarrow H_2O_{\ (gas)} + e^- \quad (7)$$

$$H_{2\ (adsorbed)} + O^{2-}_{\ (lattice)} \rightarrow H_2O_{\ (gas)} + 2e^- \quad (8)$$

In the case of ZnO nanostructures, electrons are also extracted from the interstitial zinc atoms which act as electron donors [47]. The interstitial zinc atoms are thus ionized via the following reversible reaction:

$$Zn_i^+ \leftrightarrow Zn_i^{2+} + e^- \quad (9)$$

(Kröger–Vink notation [48])

This discussion explains the mechanism that governs the ZnO nanohexagones sensors. For n-type ZnO crystals, the intrinsic carrier concentration is mainly determined by deviations from stoichiometry, usually in the form of interstitial zinc and oxygen vacancies, which act as electron donors [49]. The conduction electrons coming from the point defects play a crucial role in gas sensing of metal oxides. Consequently, the electrical conductivity of ZnO nanostructures strongly depends on the surface states created by molecular adsorption that results in depletion layer and band modulation [50].

Nanostructured metal oxides conductivity is strongly influenced by their overall surface stoichiometry.

The charge carriers depletion affects the superficial layer of the metal oxide structure and this explains why nanostructured films are much more responsive than thin film based sensors. As for the case of nanocrystallites size [51], also for nanohexagones some geometrical aspects are important. Mono-dimensional and bi-dimensional nanostructures' sensing properties are affected differently because of their different cross-section. If we assume it as cylindrical, the response of a single nanowire goes as

$$\text{Response proportional to } r^2/(r-l)^2 \quad (10a)$$

where r is the nanowire radius and l is the depletion layer thickness. The response of a nanohexagone or any other two-dimensional nanostructure goes instead as

$$\text{Response proportional to } r/(r-l) \times L/(L-2l) \quad (10b)$$

where r is the nanohexagone thickness and L its width. Eq. (10b) simplifies in

$$\text{Response proportional to } r/(r-l) \quad (10c)$$

when $L \gg l$ (which is true in the case of nanohexagones). This means that at very low scale, when $r \approx l$, the response of a mono-dimensional nanostructure raises higher than that of a two-dimensional counterpart. On the other hand, the two-dimensional shape of nanohexagones gives them great advantages: faster response and recovery times and lower LoD. As shown in Tables 1 and 2, both response and recovery times are much faster than those found for one-dimensional based sensors. This can be

explained with the higher surface-to-volume of the hexagonal sheets, which allows them to respond as a whole in a faster way. The larger cross-section of the two-dimensional nanostructures leads also to a higher base current, which leads to a lower limit of detection. These characteristics make nanohexagones (or other two-dimensional nanostructures whose thickness is comparable with the depletion layer) better candidate to gas sensing than mono-dimensional nanostructures.

5. Conclusions

In summary, a large forest of ZnO hexagonal nanostructures has been grown and a H_2 sensor has been fabricated. The nanohexagones show a large surface-to-volume ratio. Gas sensing performance is optimized at the low working temperature of 175 °C, with a sensor response of 5.37 for 500 ppm of H_2. Response and recovery time are fast ($<$ 18 s for every concentration in the range) and the devices show good reversibility. Furthermore, the devices show a remarkably low limit of detection (lower than 200 ppb). Such small value is due to the different geometry and dimensionality of the sensing nanostructure from its nanowire-based competitors.

Acknowledgments

The authors would like to thank C. Armellini and L. Toniutti for their helpful support with XRD measurements and secondary electron microscopy work, respectively.

Appendix. Supporting information

Supplementary data associated with this article can be found in the online version at http://dx.doi.org/10.1016/j.talanta.2014.01.051.

References

[1] J. Chou, Hazardous Gas Monitors: A Practical Guide to Selection, Operation, and Application, McGraw-Hill, New York, 1999.
[2] P. Moriarty, D. Honnery, Int. J. Hydrogen Energy 34 (2009) 31–39.
[3] R. Chaubey, S. Sahu, O.O. James, S. Maity, Renew. Sustain. Energy Rev. 23 (2013) 443–462.
[4] Jing-Yao Zhang, Chang Liu, Lei Zhou, Kai Qu, Ruitao Wang, Ming-hui Tai, Ji-chao Wei Lei, Qi Fei Wu, Zhi-xin Wang, Hepato-Gastroenterol. 59 (2012) 1026–1032.
[5] M. Shahid, N. Bidin, Y. Mat, M.I. Ullah, J. Energy Resour. Technol. 134 (2012) 034002.
[6] T. Seiyama, Chemical Sensor Technology, Elsevier, Amsterdam, The Netherlands, 1990.
[7] G. Korotcenkov, B.K. Cho, Sens. Actuators B 188 (2013) 709–728.
[8] T. Seiyama, A. Kato, K. Fujishi, M. Nagatani, Anal. Chem. 34 (1962) 1502–1503.
[9] G. Ciofani, G.G. Genchi, V. Mattoli, Mater. Sci. Eng. C 32 (2012) 341–347.
[10] A. Wei, L. Pan, W. Huang, Mater. Sci. Eng. B – Adv. 176 (2011) 1409–1421.
[11] D. Panda, T. Tseng, J. Mater. Sci. 48 (2013) 6849–6877.
[12] E. Comini, G. Faglia, G. Sberveglieri, Z. Pan, Z.L. Wang, Appl. Phys. Lett. 81 (2002) 1869–1871.
[13] G. Korotcenkov, B.K. Cho, Prog. Cryst. Growth 58 (2012) 167–208.
[14] N. Ramgir, N. Datta, M. Kaur, S. Kailasaganapathi, A.K. Debnath, D.K. Aswal, S. K. Gupta, Colloids Surf. A 439 (2013) 101–116.
[15] M. Tonezzer, N.V. Hieu, Sens. Actuators B 163 (2012) 146–152.
[16] J.J. Hassan, M.A. Mahdi, C.W. Chin, H. Abu-Hassan, Z. Hassan, Sens. Actuators B 176 (2013) 360–367.
[17] C. Agashe, M.G. Takawale, B.R. Marathe, V.G. Bhide, Sol. Energy Mater. 17 (1988) 99–117.
[18] J.F. Moudler, W.F. Stickle, P.E. Sobol, K.D. Bomben, Handbook of X-ray Photoelectron Spectroscopy, Physical Electronics, Inc., Eden Prairie (1995) 88.
[19] A. Kolmakov, Y. Zhang, G. Cheng, M. Moskovits, Adv. Mater. 15 (2003) 997–1000.
[20] S. Ahlers, G. Muller, T. Doll, Sens. Actuators B 107 (2005) 587–599.
[21] L. Bie, X. Yan, J. Yin, Y. Duan, Z. Yuan, Sens. Actuators B 126 (2007) 604–608.
[22] G. Sakai, N. Matsunaga, K. Shimanoe, N. Yamazoe, Sens. Actuators B 80 (2001) 125–131.
[23] N.L. Hung, E. Ahn, S. Park, H. Jung, H. Kim, S. Hong, D. Kim, J. Vac. Sci. Technol. A 27 (2009) 1347–1351.
[24] A. Qurashi, N. Tabet, M. Faiz, T. Yamzaki, Nanoscale Res. Lett. 4 (2009) 948–954.
[25] A. Qurashi, M. Faiz, N. Tabet, M.W. Alam, Superlattices Microstruct. 50 (2011) 173–180.
[26] R. Khan, H.W. Ra, J.T. Kim, W.S. Jang, D. Sharma, Y.H. Im, Sens. Actuators B 150 (2010) 389–393.
[27] Q. Ahsanulhaq, J.H. Kim, J.S. Lee, Y.B. Hahn, Electrochem. Commun. 12 (2010) 475–478.
[28] Z.H. Lim, Z.X. Chia, M. Kevin, A.S. Wong, G.W. Ho, Sens. Actuators B 151 (2010) 121–126.
[29 J.X. Wang, X.W. Sun, Y. Yang, H. Huang, Y.C. Lee, O.K. Tan, L. Vayssieres, Nanotechnology 17 (2006) 4995–4998.
[30 P. Wadkar, D. Bauskar, P. Patil, Talanta 105 (2013) 327–332.
[31 O. Lupan, G. Chai, L. Chow, Microelectron. Eng. 85 (2008) 2220–2225.
[32] O. Lupan, G. Chai, L. Chow, Microelectron. J. 38 (2007) 1211–1216.
[33] O. Lupan, L. Chow, T. Pauporté, L.K. Ono, B. Roldan Cuenya, G. Chai, Sens. Actuators B 173 (2012) 772–780.
[34] O. Lupan, V.V. Ursaki, G. Chai, L. Chow, G.A. Emelchenko, I.M. Tiginyanu, A. N. Gruzintsev, A.N. Redkin, Sens. Actuators B 144 (2010) 56–66.
[35] B. Huang, J. Lin, Appl. Surf. Sci. 280 (2013) 945–949.
[36] S.K. Hazra, S. Basu, Sens. Actuators B 117 (2006) 177–182.
[37] N.H. Al-Hardan, M.J. Abdullah, A. Abdul Aziz, Int. J. Hydrogen Energy 35 (2010) 4428–4434.
[38] J.J. Hassan, M.A. Mahdi, S.J. Kasim, N.M. Ahmed, H.A. Hassan, Z. Hassan, Mater. Sci. – Pol. 31 (2013) 180–185.
[39] I. Mora-Seró, F. Fabregat-Santiago, J. Denier, B. Bisquert, R. Tena-Zaera, J. Elias, C. Lévy-Clémen, Appl. Phys. Lett. 89 (2006) 203117.
[40] G. Neri, A. Bonavita, G. Micali, G. Rizzo, E. Callone, G. Carturan, Sens. Actuators B 132 (2008) 224–233.
[41] J.H. Park, J.H. Lee, Sens. Actuators B 136 (2009) 224–229.
[42] J.X. Wang, X.W. Sun, Y. Yang, H. Huang, Y.C. Lee, O.K. Tan, L. Vayssieres, Nanotechnology 17 (2006) 4995–4998.
[43] S.A. Anggraini, M. Breedon, N. Miura, J. Electrochem. Soc. 160 (2013) B164–B169.
[44] S. Wang, P. Wang, C. Xiao, B. Yao, R. Zhao, M. Zhang, CrystEngComm 15 (2013) 9170.
[45] H. Windischmann, P. Mark, J. Electrochem. Soc. 126 (1979) 627–633.
[46] O. Coban, S. Tekmen, S. Tuzemen, Sens. Actuators B 186 (2013) 781–788.
[47] M. Takata, D. Tsubone, H. Yanagida, J. Am. Ceram. Soc. 59 (1976) 4–8.
[48] ⟨http://en.wikipedia.org/wiki/Kroger-Vink_notation⟩.
[49] Z.M. Jarzebski, Oxide Semiconductors, Pergaman Press, Oxford, New York, 1973.
[50] H. Windischmann, P. Mark, J. Electrochem. Soc. 126 (1979) 627–633.
[51] S. Seal, S. Shukla, JOM, The Journal of The Minerals, Metals & Materials Society. 54 (2002) 35–38.